

# A continuous symmetry breaking measure for finite clusters using Jensen-Shannon divergence

Ling Lan<sup>1</sup>      Qiang Du<sup>2</sup>      Simon J. L. Billinge<sup>1</sup>

<sup>1</sup>Department of Applied Physics and Applied Mathematics, Columbia University, New York, NY 10027, USA

<sup>2</sup>Department of Applied Physics and Applied Mathematics, and Data Science Institute, Columbia University, NY 10027, USA

## Abstract

A quantitative measure of symmetry breaking is introduced that allows the quantification of which symmetries are most strongly broken due to the introduction of some kind of defect in a perfect structure. The method uses a statistical approach based on the Jensen-Shannon divergence. The measure is calculated by comparing the transformed atomic density function with its original. Software code is presented that carries the calculations out numerically using Monte Carlo methods. The behavior of this symmetry breaking measure is tested for various cases including finite size crystallites (where the surfaces break the crystallographic symmetry), atomic displacements from high symmetry positions, and collective motions of atoms due to rotations of rigid octahedra. The approach provides a powerful tool for assessing local symmetry breaking and offers new insights that can help researchers understand how different structural distortions affect different symmetry operations.

## 1 Introduction

Symmetry is a fundamental property in the analysis of systems ranging from particle physics to condensed matter materials, including crystals, molecules, and polymers, among others [17, 8]. The role of symmetry breaking (SB) is equally significant, as it is closely associated with many critical phenomena in physics and material science, and has been extensively studied over the past decades [1, 13]. Traditionally, material symmetry has been viewed as a dichotomous concept, where a cluster of atoms either satisfies or violates a symmetry operation. Based on this understanding, symmetry finders have been developed to identify whether a given structure is invariant under certain transformations within a global tolerance [10, 22].

In nanomaterials, the structures tend to be complex and length-scale dependent. In general, we would like to explore the concept of distance-dependent point symmetry because local symmetry can differ from average symmetry, for example, due to the

averaging of local symmetry broken distortions over multiple allowed variants [20, 3, 29, 27]. In this case, some symmetries may be absolutely or approximately preserved by the averaging whereas other symmetries are significantly broken. This raises new questions that are not addressed by the dichotomous view of material symmetry. For example, one may inquire about the extent and manner in which material properties are altered when symmetries are only approximately broken. In this case, we may be able to ignore the weak breaking of some symmetries in our analysis of the material, but not ignore others that have a stronger effect on the properties. Additionally, it may be of interest to determine which symmetry operations are significantly or only approximately violated by a specific structural distortion. To address this issue, we aim to develop a quantitative, rather than categorical, measure of SB that bridges the gap between satisfying and violating symmetries.

The concept of creating a continuous SB measure for material structures and molecular systems has long been a subject of interest. For example, Zabrodsky et al. [28], and the software based on their method [24], define a continuous measure as the minimal distance between a given structure and a structure with the desired symmetry. They first scan all relevant permutations to find the reference structure with the desired symmetry and then calculate the measure as the squared error of the coordinates. Similar methods have been applied in other studies [11, 12]. However, this approach has two main limitations: the number of permutations increases significantly for larger structures, and it only considers atomic coordinates, ignoring other particle properties. In contrast, our paper introduces a continuous SB measure from a statistical perspective. We avoid the search for the desired structure by adopting a continuous representation of finite clusters. And this measure not only accounts for the positions of particles but also incorporates atomic species, occupancy, and atomic distributions through thermal vibrations.

Our statistical symmetry breaking measure (SBM),  $\mathcal{S}_{T_\alpha}$ , uses information theory to quantify symmetry loss in a finite atomic cluster under a transformation  $T_\alpha$ . The cluster is represented by a normalized electron-weighted density function  $\mu$ . The measure is defined as the Jensen-Shannon (JS) divergence [15] between the transformed density  $T_\alpha[\mu]$  and the original  $\mu$ , providing a quantitative assessment of the structure's deviation from the symmetry element  $T_\alpha$ . The measure can be computed for any operation in any atomic cluster. For an undistorted crystal structure, it returns zero for each crystallographic symmetry operation by design. However, with finite size clusters whose shape breaks symmetry, unit cell distortions, or atomic displacements, it yields a positive value that indicates the degree of SB with respect to each symmetry operation.

In this paper, we derive this measure and conduct numerical tests to evaluate its behavior for different cases, comparing it with another related SBM based on the Kullback-Leibler (KL). We demonstrate that these measures are useful for investigating factors affecting SB, such as boundary shape, perturbation size, and which atom is distorted. They also help identify which symmetries are most violated or preserved when a cluster experiences a specific distortion.

## 2 KL and JS divergences in symmetry breaking

Transform Information (TI) has been employed as a quantitative measure of SB, with successful applications in fields such as biological systems [6], and it has been demonstrated to be a general form of many classical information measures [25]. The fundamental idea behind this approach is to compare an object of interest with a transformed version of itself. The TI associated with the transformation  $T_\alpha$  is defined as

$$\mathcal{S}_{T_\alpha} = \int_D \mu(\zeta) \ln \left( \frac{\mu(\zeta)}{T_\alpha \mu(\zeta)} \right) d\zeta, \quad (1)$$

where  $\mu(\zeta)$  is an intensity function of interest over the domain  $D$ . The transformation  $T$  is parameterized by a continuous variable  $\alpha$ , such as the angle of rotation around a fixed axis. When  $\mu$  is a probability measure, TI becomes a special case of the Kullback-Leibler (KL) divergence [14], also known as relative entropy. The KL divergence, denoted by  $D_{\text{KL}}(P \parallel Q)$ , quantifies the information loss if one probability distribution  $P$  is approximated by another,  $Q$ . For the case of a continuous random variable, it is defined as

$$D_{\text{KL}}(P \parallel Q) = \int_{\mathcal{X}} p(x) \log \frac{p(x)}{q(x)} dx, \quad (2)$$

where  $p$  and  $q$  denote the probability densities of  $P$  and  $Q$ , respectively, defined on measurable space  $\mathcal{X}$ . While the KL divergence possesses the capability to quantify the distance between two probability distributions, it is not mathematically recognized as a valid metric. Specifically, it fails to satisfy the triangle inequality and lacks symmetry. Additionally, it is not always well-defined and could become unbounded. An alternative is the Jensen-Shannon (JS) divergence, given by:

$$\begin{aligned} D_{\text{JS}}(P, Q) &= \frac{1}{2} D_{\text{KL}}(P \parallel M) + \frac{1}{2} D_{\text{KL}}(Q \parallel M) \\ &= \frac{1}{2} \int_{\mathcal{X}} p(x) \log \frac{p(x)}{m(x)} + \frac{1}{2} \int_{\mathcal{X}} q(x) \log \frac{q(x)}{m(x)} dx, \end{aligned} \quad (3)$$

where  $M$  represents a mixture distribution of  $P$  and  $Q$ , defined as  $M = \frac{1}{2}P + \frac{1}{2}Q$ . Consequently, the JS divergence is often referred to as the “total divergence to the average.” When the logarithm’s base is 2, the JS divergence remains bounded by 1 [15].

Here we study measures of SB based on both the KL and JS divergences and apply them to model systems to understand their behavior.

## 3 A symmetry breaking measure for finite clusters

### 3.1 Finite cluster representation

In our proposed model, we represent a finite cluster of atoms as a normalized electron-weighted atomic density function  $\mu(x) : x \in \mathbb{R}^3 \rightarrow \mathbb{R}$ . The electron density at each

atom is assumed to be located at the position of the atomic nucleus. However, due to atomic motions, the probability distribution of the atomic density can be approximated by a three-dimensional Gaussian distribution, commonly known as the Debye-Waller approximation [26], weighted by the number of electrons held by the atom. Specifically, for any atom  $k$  where the average location of the nucleus is at  $\mathbf{x}_k$ , the electron-weighted atomic density can be written as

$$\tilde{\mu}_k = e_k \cdot o_k \cdot \mathcal{N}(\mathbf{x}_k, \mathbf{U}_k), \quad (4)$$

where,  $e_k$  denotes the number of electrons held by atom  $k$ ,  $o_k$  is its occupancy factor, and  $\mathbf{U}_k \in \mathbb{R}^{3 \times 3}$  is the anisotropic atomic displacement tensor (ADT). For simplicity, here we treat this distribution as being isotropic, that is,  $\mathbf{U}_k = U_k \mathbf{I}_3$  is a diagonal matrix, and all the diagonal entries,  $U_k$ , are equal to the  $U_{\text{iso}}$  of atom  $k$ . Here  $U_k = 1/3 \times (\mathbf{U}_{k,11} + \mathbf{U}_{k,22} + \mathbf{U}_{k,33})$  can be interpreted as a mean-square displacement averaged over all the three directions [23].

With this representation, the electron-weighted atomic density function of a finite cluster of particles can be expressed as the superposition of Gaussian distributions,

$$\tilde{\mu} = \sum_{k=1}^N \tilde{\mu}_k = \sum_{k=1}^N \tilde{\phi}_k \mathcal{N}(\mathbf{x}_k, U_k \mathbf{I}_3), \quad (5)$$

where  $\tilde{\phi}_k = e_k \cdot o_k$ . To transform the electron-weighted atomic density function into a probability density function, we normalize  $\tilde{\mu}$  such that it possesses an  $L_1$  norm of unity. This results in the normalized electron-weighted atomic density function,

$$\mu = \frac{\tilde{\mu}}{\|\tilde{\mu}\|_{L_1}} = \frac{\tilde{\mu}}{\sum_{k=1}^N \tilde{\phi}_k} = \sum_{k=1}^N \phi_k \mathcal{N}(\mathbf{x}_k, U_k \mathbf{I}_3), \quad (6)$$

where  $\phi_k = \tilde{\phi}_k / \sum_{i=1}^N \tilde{\phi}_i$ . For the case of isotropic ADTs, a transformation  $T_\alpha$  to  $\mu$  is equivalently defined by transforming the Gaussian mean of all the particles,

$$\begin{aligned} T_\alpha[\mu] &= T_\alpha \left[ \sum_{k=1}^N \phi_k \mathcal{N}(\mathbf{x}_k, U_k \mathbf{I}_3) \right] \\ &= \sum_{k=1}^N \phi_k \mathcal{N}(T_\alpha[\mathbf{x}_k], U_k \mathbf{I}_3). \end{aligned} \quad (7)$$

### 3.2 Symmetry breaking measure

Using our finite cluster representation, given a general transformation  $T_\alpha$ , we first define the SBM based on the KL divergence (KL-SBM),  $\mathcal{S}_{T_\alpha}^{KL}[\mu]$ , as

$$\begin{aligned} \mathcal{S}_{T_\alpha}^{KL}[\mu] &= D_{\text{KL}}(\mu \| T_\alpha[\mu]) \\ &= \int_{\mathbb{R}^3} \mu(x) \log \left( \frac{\mu(x)}{T_\alpha[\mu](x)} \right) dx. \end{aligned} \quad (8)$$

This measure quantifies the similarity of the structure with itself after the transformation of interest  $T_\alpha$ . We will explore the performance of this measure in simple cases below.

Although  $\mathcal{S}_{T_\alpha}[\mu]$  is bounded for Gaussian mixtures [18], the bounding limit is contingent upon specific attributes of the finite cluster, including atom species and the number of atoms incorporated. As a consequence, generalization to compare the relative SB of dissimilar clusters is not possible.

We also define a SBM based on the JS divergence which we might expect to give a more transferrable measure bound. We define the the JS-SBM,  $\mathcal{S}_{T_\alpha}^{JS}[\mu]$ , as

$$\mathcal{S}_{T_\alpha}^{JS}[\mu] = \frac{1}{2} \int_{\mathcal{X}} \mu(x) \log \frac{\mu(x)}{m(x)} + \frac{1}{2} \int_{\mathcal{X}} T_\alpha[\mu](x) \log \frac{T_\alpha[\mu](x)}{m(x)} dx, \quad (9)$$

where  $m$  is an equal mixture of  $\mu$  and  $T_\alpha[\mu]$ . Specifically,

$$m = \sum_{k=1}^N \frac{\phi_k}{2} [\mathcal{N}(\mathbf{x}_k, U_k \cdot \mathbf{I}_3) + \mathcal{N}(T_\alpha[\mathbf{x}_k], U_k \cdot \mathbf{I}_3)]. \quad (10)$$

$\mathcal{S}_{T_\alpha}^{KL}[\mu]$  and  $\mathcal{S}_{T_\alpha}^{JS}[\mu]$  both satisfy the three divergence properties:

- Self similarity:  $\mathcal{S}_{T_\alpha}[\mu] = 0$  if  $T_\alpha$  is the identity.
- Self identification:  $\mathcal{S}_{T_\alpha}[\mu] = 0$  only if  $T_\alpha[\mu] = \mu$ .
- Positivity:  $\mathcal{S}_{T_\alpha}[\mu] \geq 0$  for all  $\mu$ , given any transformation  $T_\alpha$ .

The first two properties can be succinctly stated as  $\mathcal{S}_{T_\alpha}[\mu] = 0$  if and only if the  $T_\alpha$  transformation is a symmetry preserving operation,  $\mathcal{O}$ , of the structure. In other words,

$$\mathcal{S}_{\mathcal{O}}[\mu] = 0. \quad (11)$$

In all other cases,  $\mathcal{S}_{T_\alpha}[\mu]$  is positive.

For the case of the JS-SBM, when using a logarithm with a base of 2 in Eq. 9, it is bounded by one. If the natural logarithm is employed, the upper bound becomes  $\sqrt{2}$ .  $\mathcal{S}_{T_\alpha}^{JS}[\mu]$  reaches its upper bound if and only if  $\mu$  and  $T_\alpha$  are disjoint, indicating that the operation  $T_\alpha$  is broken completely. For a Gaussian mixture  $\mu$ , which is consistently non-zero, this upper bound will not be realized. However, if  $\mathbf{x}_k$  and all  $T_\alpha[\mathbf{x}_k]$  are sufficiently distant in terms of their  $U_{\text{iso}}$ 's,  $\mathcal{S}_{T_\alpha}^{JS}[\mu]$  can approach close to its bound.

A small but non-zero  $\mathcal{S}_{T_\alpha}[\mu]$  indicates the transformation  $T_\alpha$  is only weakly breaking the symmetry. In this context,  $\mathcal{S}_{T_\alpha}[\mu]$  is a continuous measure of structural SB. If a structure undergoes a small distortion, for example, due to the displacement of one or several atoms off crystallographic special positions by a small magnitude, the SBM can be calculated for each symmetry operation of the undistorted structure to identify the symmetry operations that have been more severely disrupted, those that remain intact, and those that have been marginally affected.

For a high-symmetry heterostructure, such as an infinite crystal with a Face-Centered Cubic (FCC) lattice of nickel, we refer to a set of symmetry operations

denoted as  $\mathcal{T} = \{T_i\}$ , which contains transformations capable of yielding an identical object after carried out. We then introduce some changes to this heterostructure. This results in the object losing some of the symmetry operations from its set (and in principle, possibly gaining some new ones) and having a new set of symmetry operations,  $\mathcal{T}' = \{T'_i\}$ . Strictly speaking, SB of this structure can be defined as the condition where the SBM  $\mathcal{S}_{T_i}$  of some symmetry operation  $T_i \in \mathcal{T}$  result in  $\mathcal{S}_{T_i} > 0$ .

### 3.2.1 Symmetry breaking measure of symmetry operators

The JS-SBM and KL-SBM are formulated as continuous functions of transformations  $T_\alpha$ , such as  $R_\alpha$ , which represents a counterclockwise rotation of angle  $\alpha$ . The SBM is uniquely defined for the transformation and  $T_\alpha$  does not need to be a symmetry operation, which is defined as an action leaving an object unchanged.

Determining the SBM of *symmetry operators* is not trivial, because the *symmetry operators* can generate more than one symmetry operation. For example, such as the proper axes of rotation  $C_n$  can lead to  $n - 1$  operations, specifically  $C_n, C_n^2, \dots, C_n^{n-1}$ .  $C_n^n$  is considered the “identity” operation, denoted  $E$ . For example, in structures with  $n$ -fold rotational symmetry  $C_n$ , the SBM for these operations are zero ( $\mathcal{S}_{C_n} = \mathcal{S}_{C_n^2} = \dots = \mathcal{S}_{C_n^{n-1}} = 0$ ). However, if a perturbation disrupts this  $n$ -fold symmetry, the SBM for  $C_n^i$  and  $C_n^j$  may differ for some  $i, j \in \{1, \dots, n - 1\}$ . Therefore, we need a measure to quantify how much a particular symmetry operator, such as  $n$ -fold rotation, is broken by a symmetry lowering distortion.

To address this, we introduce *symmetry breaking measure of operators*,  $\mathcal{S}_\mathcal{O}$ , as the average SBM of all the  $\{\mathcal{O}^i\}$  operations derived from  $\mathcal{O}$ .

$$\mathcal{S}_\mathcal{O} = \frac{1}{|\{\mathcal{O}^i\}|} \sum_{\mathcal{O}^i} \mathcal{S}_{\mathcal{O}^i}. \quad (12)$$

For example  $\mathcal{S}_{C_4} = 1/3 \sum_{i=1}^3 \mathcal{S}_{C_4^i}$ . This measure gives a value of 0 when symmetry is preserved, but ranges between 0 and 1 for the JS-SBM if symmetry is partially broken.

### 3.2.2 Symmetry breaking measure of a single-atom system

To gain insights, we will consider a structure with a single-atom in the unit cell with  $U_{\text{iso}} = U$  and which becomes displaced by  $\mathbf{d}$ . We have

$$\mu(\mathbf{x}) = \mathcal{N}(\mathbf{x}; \boldsymbol{\mu}, U\mathbf{I}_3), \quad (13)$$

$$T_{\mathbf{d}}[\mu](\mathbf{x}) = \mathcal{N}(\mathbf{x}; \boldsymbol{\mu} + \mathbf{d}, U\mathbf{I}_3). \quad (14)$$

In this simple case there is an analytic expression for the the KL-SBM,

$$\mathcal{S}_{T_{\mathbf{d}}}^{KL} = D_{\text{KL}}(\mu \| T_{\mathbf{d}}[\mu]) = \frac{d^2}{2U}, \quad (15)$$

where  $d = \|\mathbf{d}\|_{L_2}$  is the displacement distance. Details of the derivation can be found in the supplemental materials. This result suggests that for small distortions  $\mathbf{d}$ , the

KL-SBM increases with the square of the displacement  $d^2$ , demonstrating a sensitive measure of even minor positional changes.

The  $\mathcal{S}_{T_d}^{JS}[\mu]$  case will be more challenging because it involves a Gaussian mixture  $m = \frac{1}{2}\mu + \frac{1}{2}T_d[\mu]$ . We compute this numerically and show the result in Figure 1(a) for various values of  $U_{\text{iso}}$ . The JS-SBM increases approximately quadratically with increasing  $d$ . As we might expect, it goes up more slowly when  $U_{\text{iso}}$  is larger. In Figure 1(b), we consider a threshold value of  $d$  at which the JS-SBM reaches 0.1 and plot this as a function of  $U_{\text{iso}} = U$ . The slope of the plot indicates that achieving a JS-SBM of 0.1 requires an approximate increase of 0.03 Å in the displacement magnitude  $d$  for every 0.01 Å<sup>2</sup> increase in  $U$ .

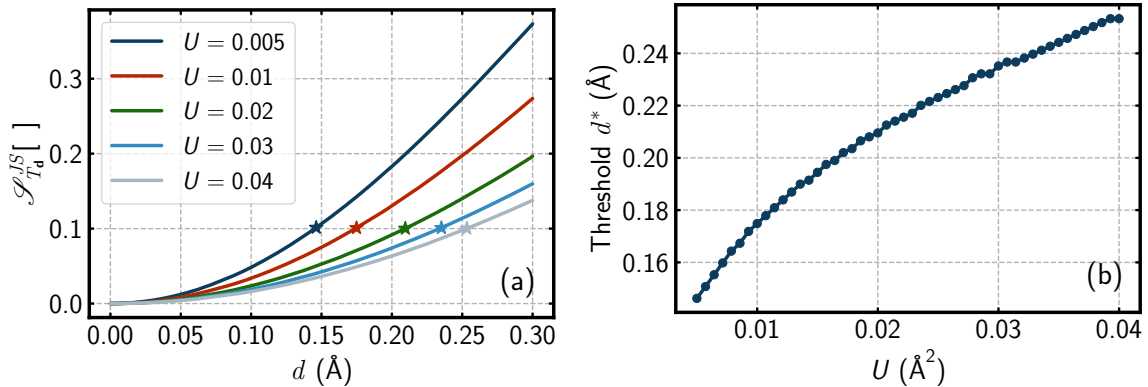


Figure 1: (a) The JS-SBM of the translational symmetry when an atom is displaced by  $d$  from itself, plotted for atoms with different  $U_{\text{iso}}$ . The star on each curve represents the point at which the JS-SBM reaches 0.1. (b) The value of  $d^*$  where the JS-SBM first reaches the 0.1 threshold for different  $U_{\text{iso}}$ .

## 4 Numerical Methods

Here we discuss methods for computing the SBM. Neither the KL or JS divergences have closed-form expressions for Gaussian Mixture Models. In this case, Monte Carlo (MC) simulation emerges as a useful technique for estimating  $D_{\text{KL/JS}}(f||g)$  with arbitrary accuracy [9]. In this section, our focus is primarily on outlining the method to approximate  $\mathcal{S}_{T_\alpha}^{KL}[\mu]$  and determine the appropriate sample size for the MC simulation, contingent upon a set confidence level and a predetermined tolerance for estimation inaccuracies. The results are relevant also for  $\mathcal{S}_{T_\alpha}^{JS}[\mu]$  which is computed by combining two distinct KL-divergence computations.

The MC simulation expresses the KL divergence as the expectation of  $\log(f/g)$ ,

under the probability density function  $f$ . In other words,

$$\begin{aligned}\mathcal{S}_{T_\alpha}^{KL}[\mu] &= \int_{\mathbb{R}^3} \mu(x) \log \frac{\mu(x)}{T_\alpha[\mu](x)} dx \\ &= \mathbb{E}_{x \sim \mu} \left[ \log \frac{\mu(x)}{T_\alpha[\mu](x)} \right].\end{aligned}\tag{16}$$

The MC methodology can then be applied to estimate the expectation values using the algorithm,

---

**Algorithm 1** The Monte Carlo estimation of  $\mathcal{S}_{T_\alpha}^{KL}[\mu]$

---

1. Draw  $M$  independent and identically distributed (i.i.d.) samples  $x_i$  from the probability density function  $\mu$ .
  2. Compute  $(\mathcal{S}_{T_\alpha}^{KL})^{MC}[\mu] = \frac{1}{M} \sum_{i=1}^M h(x_i)$ , where  $h(x_i) = \left[ \log \left( \frac{\mu(x_i)}{T_\alpha[\mu](x_i)} \right) \right]$ .
- 

By the law of large numbers, the MC estimate  $(\mathcal{S}_{T_\alpha}^{KL})^{MC}[\mu]$  converges to  $\mathcal{S}_{T_\alpha}^{KL}[\mu]$  as the number of samples  $M \rightarrow \infty$ . The estimation error is of order  $O(1/\sqrt{M})$ . One can construct a confidence interval for the MC estimate as

$$CI = \left( (\mathcal{S}_{T_\alpha}^{KL})^{MC}[\mu] - z \frac{\sigma}{\sqrt{M}}, (\mathcal{S}_{T_\alpha}^{KL})^{MC}[\mu] + z \frac{\sigma}{\sqrt{M}} \right),\tag{17}$$

where  $\sigma$  is the standard deviation of  $\{h(x_i)\}_{i=1}^M$ , and  $z$  is the  $z$ -score determined by the confidence level. For instance, for a 95% confidence interval, implying a 95% chance of containing the true value of  $\mathcal{S}_{T_\alpha}[\mu]$ ,  $z$  is approximately equal to 1.96. One can estimate the required sample size  $M$  using the following algorithm:

---

**Algorithm 2** Estimation of Monte Carlo sample size  $M$

---

1. Choose an arbitrary large  $M'$ , and draw  $M'$  i.i.d. samples  $x_i$  from  $\mu$ .
  2. Compute  $\sigma^2 = \text{Var}(h(x_i))$ , where  $h(x_i) = \left[ \log \left( \frac{\mu(x_i)}{T_\alpha[\mu](x_i)} \right) \right]$ .
  3. The recommended sample size  $M$  is  $(z \cdot \sigma/\epsilon)^2$ , where  $\epsilon$  is the error tolerance on each side.
- 

For example, the minimum sample size that ensures a 95% probability of the true  $\mathcal{S}_{T_\alpha}^{KL}[\mu]$  being within  $CI = ((\mathcal{S}_{T_\alpha}^{KL})^{MC}[\mu] \pm \epsilon)$  is  $(1.96 \cdot \sigma/\epsilon)^2$ . Increasing the value of  $M'$  in Algorithm 2 improves the accuracy of the estimated standard deviation  $\sigma$ , thereby leading to a more precise estimation of the sample size  $M$ .

The JS divergence, which averages two KL-divergences, can be calculated following Algorithm 1 by applying it separately to each component. Similarly, the confidence interval and required sample size for each estimation can be derived using Algorithm 2. Notably, due to the interdependence of the two distributions, the confidence interval for their combined sum cannot be obtained by simply merging the individual confidence intervals.



## 5 Numerical Results

This section discusses how the SBM quantitatively analyzes distortions in finite clusters. When focusing on local distortions, we often examine smaller, locally distorted segments within larger structures. Here, we present two finite clusters as examples, each a segment cut from infinite crystal structures, to demonstrate the practical use of SBM for local distortion analysis. The first cluster, discussed in Section 5.1, is taken from an FCC Nickel crystal structure. Its high inherent symmetry makes it ideal for evaluating how SBM detects symmetry violations. We also examine how different structural cutout choices introduce SB, as described in Section 5.1.1. The second example involves a supercell derived from a distorted perovskite with octahedral tilts, detailed in Section 5.2. This case illustrates how SBM enables dynamic analysis of distortion processes by tracking SBM as the perovskite transitions from its original, undistorted state to one with octahedral tilts.

### 5.1 The violation of symmetry elements of local distorted Nickel

#### 5.1.1 The symmetry breaking from the boundary of the finite cluster

Here we explore how the SBM behaves under different situations. We begin with finite clusters of atoms that are cut out from larger bulk crystals. This simulates idealized nanoparticles where there are no local atomic displacements or relaxations except for the finite size of the particle. This is not different from a point-group symmetry analysis of discrete molecules. However, we are interested in this as an illustrative example of quantifying the SBM inherent in the nanosizing.

**Test Design** In our exploration, we create finite chunks of material where the particle shape either preserves or breaks the underlying symmetry, and we delve into each scenario. We investigate a counterclockwise rotation operation  $R_\alpha$  along the 4-fold symmetry axis of the face-centered cubic (FCC) nickel structure, considering spherical and cubic cutouts (point-symmetry-preserving), as well as spheroidal and rectangular cutouts (symmetry-lowering):

- **Spherical Cutout:** Contains all atoms within a distance of one lattice parameter from the central nickel atom.
- **Cubic Solid Cutout:** Has a side length of one lattice parameter, forming a regular unit cell of nickel.
- **Spheroidal Cutout:** Centered on a central atom, extending two unit cells along the major axis and one unit cell along each minor axis, containing all atoms within this volume.
- **Rectangular Solid Cutout:** Encompasses two adjacent unit cells.

The rotation axis passes through either the central nickel atom or the cluster's center of mass (if no central atom exists) and is parallel to the positive  $c$ -axis of the original crystallographic unit cell.

In this test, the lattice parameter for nickel was chosen to be 3.52 Å. The atomic displacement parameters (ADP) for each nickel atom were set to  $U_{\text{iso}} = 0.013 \text{ \AA}^2$ . For each nickel atom, the electron count is 28, which aligns with its atomic number,  $Z$ . Additionally, the occupancy,  $o$ , is set to one for each site. For the evaluation of SBM, both  $\mathcal{S}_{R_\alpha}^{KL}[\mu]$  and  $\mathcal{S}_{R_\alpha}^{JS}[\mu]$  were estimated using Monte Carlo random sampling. The sample sizes for these estimations were determined based on a 95% confidence interval, with a bilateral error tolerance set at 0.025 for the KL-SBM and 0.0025 for the JS-SBM.

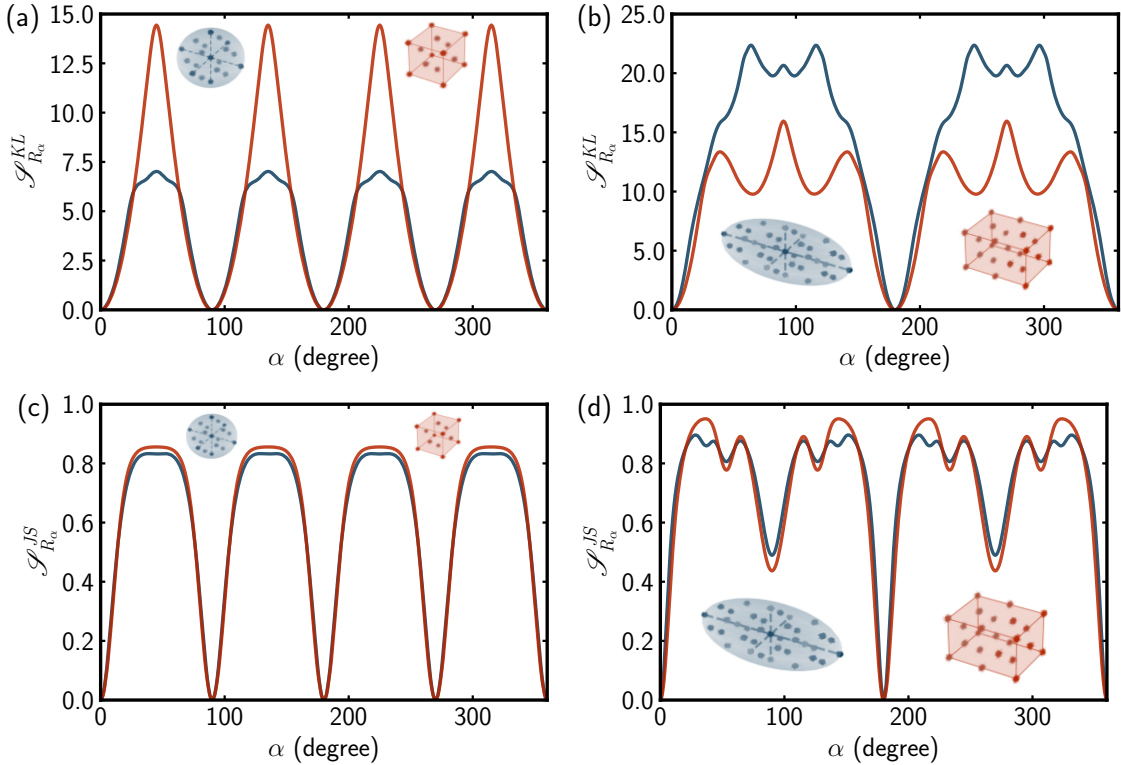


Figure 2: (a and b) The KL-SBM  $\mathcal{S}_{R_\alpha}^{KL}[\mu]$  and (c and d) the JL-SBM  $\mathcal{S}_{R_\alpha}^{JS}[\mu]$ , extracted from finite clusters of a nickel crystal structure. In subplots (a and c), spherical (blue) and cubic (red) shapes are used for cutouts, while spheroidal (blue) and rectangular (red) shapes are demonstrated in subplots (b and d). These curves depict the variation of  $\mathcal{S}_{R_\alpha}[\mu]$  as the respective cluster is rotated by angle  $\alpha$  (measured in degrees). This rotation is about an axis aligned with the crystallographic  $c$ -axis and intersects the cluster's center of mass.

**SBM for symmetry-preserving cutouts** We first consider the point-symmetry-preserving cutouts in Fig. 2 (a and c). By definition, both  $\mathcal{S}_{R_\alpha}[\mu] = 0$  when  $\alpha = 0$  as the object is compared with itself. As we rotate the angle away from zero,  $\mathcal{S}_{R_\alpha}[\mu]$

increase. Because the object has 4-fold rotational symmetry,  $C_4$ , for rotations about this axis, we expect both SBM  $\mathcal{S}_{R_\alpha} = \mathcal{S}_{C_4^i} = 0$  when  $\alpha = i\pi/2$  rad for  $i = 1, 2, 3$ , which results in  $\mathcal{S}_{R_\alpha}$  being a function with 4-fold periodicity in  $\alpha$ , as is seen. The fact that these cutouts do not break the point-symmetry is evident in the fact that  $\mathcal{S}_{R_\alpha} = 0$  for every 90 degrees of rotation, preserving the 4-fold rotational symmetry present in the underlying structure.

The two symmetry-preserving cutouts result in similar  $\mathcal{S}_{R_\alpha}^{KL}[\mu]$  trajectories for small values of  $\alpha$  away from the high symmetry points. The curves initially increase at about the same rate. Both curves go through a maximum at  $45^\circ$ , though the cubic cutout has a much higher maximum at this point. The sphere has a higher overall symmetry and this seems to result in a lower maximum of KL-SBM.

The behavior of  $\mathcal{S}_{R_\alpha}^{JS}[\mu]$  is also similar for each of these clusters at small deviations of  $\alpha$  from high symmetry points. However, the behavior of JS-SBM is notably different in the proximity of their local maxima where the two curves follow each other closely. Both trajectories rapidly approach their local maxima, approximating a value of 0.85, and subsequently remain relatively constant around the  $45^\circ$  rotation.

**SBM for symmetry-lowering cutouts** In the cases of spheroid and rectangular solid cutouts, the internal structure does not deviate from the ideal FCC nickel structure, but the shape of the cluster takes the object from 4-fold to 2-fold symmetric about this rotation axis. We therefore expect the SBM to be a 2-fold periodic function with zeros at 0 and 180 degrees of rotation. This is indeed what is seen in Fig. 2 (b and d).

Analogous to the symmetry-preserving cases, the profiles of  $\mathcal{S}_{R_\alpha}^{KL}[\mu]$  for these cutouts display pronounced discrepancies. Interestingly, in both cases, the  $90^\circ$  rotation which was a minimum and went to zero in the symmetry-preserving cutouts, is now a local maximum in the KL-SBM, and for the rectangular cutout is a global maximum. This might be expected from the point of view that the elongated structures are perpendicular at this point. However, on the other hand, the underlying structures will come into coincidence again at these points for the atoms that do overlap due to the internal four-fold symmetry of the structure, so it is not so obvious how we might expect a SBM to behave.

On the other hand, the behavior of  $\mathcal{S}_{R_\alpha}^{JS}[\mu]$  for the spheroidal and rectangular solid cutouts exhibits much more congruence. Both cutouts yield trajectories that are closely aligned with each other. In this case, the  $90^\circ$  rotation results in a local minimum in this measure. As expected, it does not go to zero, but for both cutouts, it is a local minimum with a value of around 0.5. The nonzero local minimum at  $90^\circ$  and  $270^\circ$  for JS-SBM suggest that while the cutouts disrupt  $C_4$  symmetry, the interior Nickel structure retains this symmetry to some extent.

**KL-SBM  $\mathcal{S}_{R_\alpha}^{KL}[\mu]$  v.s. JS-SBM  $\mathcal{S}_{R_\alpha}^{JS}[\mu]$**  This observation suggests that JS-SBM is less sensitive to the boundary characteristics and particle quantity within the finite cluster. Additionally, the fact that JS-SBM values range between 0 and 1 facilitates direct comparison of SB across different clusters, making JS-SBM a more standardized

metric. Consequently, the JS-SBM's consistent and straightforward behavior makes it more suitable for comparative analysis of SB between distinct clusters compared to KL-SBM. Given these insights, the subsequent focus will exclusively be on the JS-SBM.

**SBM of symmetry operators** By an inspection of the four-fold rotational symmetry,  $C_4$  was not broken at all by the cubic and spherical cutouts but it was broken by the spheroidal and rectangular cutouts. For the sphere and cube, we find that  $\mathcal{S}_{C_4} = 1/3 \sum_{i=1}^3 \mathcal{S}_{C_4^i} = 1/3 \sum_{i=1}^3 \mathcal{S}_{R_{i\pi/2}} = 0$ , and so our operator SBM correctly returns zero as expected. We find that for the spheroid,  $\mathcal{S}_{C_4}^{JS} \approx 0.33$  and for the rectangular solid cutout,  $\mathcal{S}_{C_4}^{JS} \approx 0.29$ . Thus, by the measure  $\mathcal{S}_{C_4}^{JS}$ , we may argue that for this example, the spheroid cutout breaks the symmetry approximately the same as, but slightly more strongly than, the rectangular solid cutout.

### 5.1.2 The symmetry breaking from local perturbations

We now investigate the different ways that displaced atoms contribute to SB. As an illustrative example, we will use the same cubic cutout from the Nickel structure.

**Deviation from four-fold rotational symmetry  $C_4$**  We first test the four-fold rotational symmetry element  $C_4$  that goes through the center of the cluster and is parallel to  $c$ , as previously discussed. Perturbations are introduced within the finite cluster by selecting a single atom and displacing it with a vector  $\mathbf{d}$ . We then compute the JS-SBM,  $\mathcal{S}_{C_4}^{JS}[\mu_{\mathbf{d}}]$ . The results are summarized in Fig. 3 plotted as a function of the magnitude of  $\mathbf{d}$ ,  $d = |\mathbf{d}|$ .

Displacing an atom lying on the rotation axis in a direction along the axis (top or bottom centering atom displaced along  $c$ ) does not break symmetry and  $\mathcal{S}_{C_4}^{JS}[\mu_{\mathbf{d}}] = 0$  for all  $d$  (horizontal light yellow line in Fig. 3) as expected.

We first note that the magnitudes of  $\mathcal{S}_{C_4}[\mu]$  are considerably smaller than those from the rigid rotation of the magnitudes shown in Fig. 2. This observation is reasonable since only one particle out of the ensemble of 14 undergoes displacement, while the others remain unchanged.

Displacing these same atoms with a component perpendicular to the rotation axis does break symmetry.  $\mathcal{S}_{C_4}^{JS}[\mu_{\mathbf{d}}]$  increases smoothly as shown by the light blue and light red curves in Fig. 3. It saturates to a value of 0.072 for all displacement directions. This value corresponds to the atomic density of a single atom becoming disjoint, i.e.  $1/14$ , since we have 14 atoms in the cluster. This value is reached when the atom moves far enough from its original position that it doesn't overlap with itself or any other atoms on rotation.

For displacements of atoms which are on the non-axial face centers, the SBM plateau is at 0.143 ( $\approx 2/14$ ). In this case the displaced atom is becoming disjoint with a neighboring atom and not just with itself.

We now compare in detail how the face-center atoms behave in three scenarios, for the displacement vectors being:

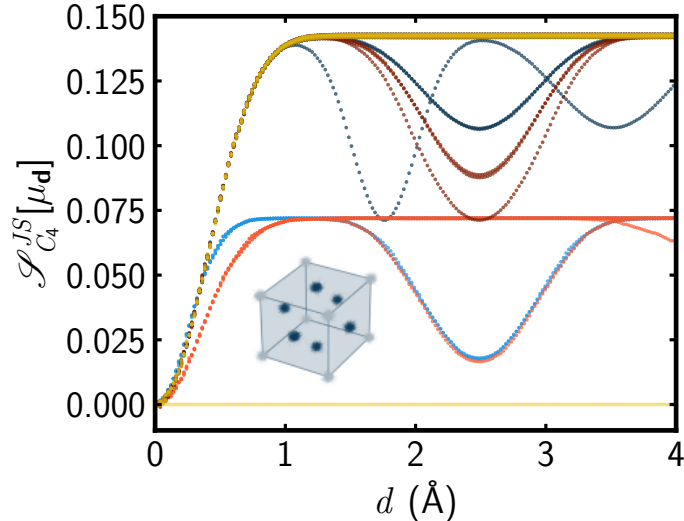


Figure 3: The SBM  $\mathcal{S}_{C_4}^{JS}[\mu_d]$  of a cubic cutout from the distorted Nickel structure. One of its face-centered atoms (darker blue atoms) is shifted parallel to the  $a$ - $b$  plane (blue), deviated from the  $a$ - $b$  plane by 45 degrees (red), or perpendicular to the  $a$ - $b$  plane (yellow). The SBM is calculated for the four-fold rotational operation  $C_4$ , whose axis passes through the center of the finite cluster, with its direction along the positive  $c$ -axis. The curves with light color represent the SBM when the top or bottom face atom is displaced, while the darker curves represents the SBM when one of the other face atoms is displaced. The figure is plotted as a function of the length of the atom displacement  $d$ .

1. parallel to  $c$  (shown in yellow).
2. within the  $a$ - $b$  plane (shown in blue) with two representative displacement directions  $(1, 0, 0)$  and  $(\sqrt{2}/2, \sqrt{2}/2, 0)$ .
3. at a  $45^\circ$  angle to the  $a$ - $b$  plane (shown in red) with directions  $(\sqrt{2}/2, 0, \sqrt{2}/2)$  and  $(1/2, 1/2, \sqrt{2}/2)$ .

All the curves smoothly increase from 0 with increasing  $d$  and eventually reach a plateau. We can gain insight into the behavior of the SBM by understanding this behavior. For the light blue curve, the atom on the rotation axis is displaced in the  $a$ - $b$  plane by a distance  $d$ . After applying the  $C_4$  symmetry operation to the displaced atom, the displacement between the original and the rotated atom is  $\sqrt{2}d$ . The SBM will have its maximum value when the displaced but unrotated atomic density no longer overlaps with the displaced but rotated atomic density, which will occur at a  $d = d^*/\sqrt{2} = 0.93/\sqrt{2}$ .

Some of the atoms remain disjoint with increasing  $d$  and  $\mathcal{S}_{C_4}^{JS}[\mu_d]$  stays on the plateau, for example, the pale red and blue curves for the  $(1,0,0)$  displacement direction. However, in other cases,  $\mathcal{S}_{C_4}^{JS}[\mu_d]$  becomes reduced with increasing  $d$ , an

apparently paradoxical result that a larger distortion results in a lower SB. The reason for this is that the displacement of the atom is so large that it starts to overlap with another atom in the structure. For example, the displacement direction of (1,1,0) of the atom at the center of the top face when it reaches the corner of the cube. Logically and mathematically this makes sense, though this does not correspond to a real situation that would be encountered in practice as it is not possible for atomic probability distributions of pairs of atoms to overlap. However, plotting  $\mathcal{S}_{C_A}^{JS}[\mu_d]$  over such and unphysically large range helps us to build intuition about the function. An analysis of SBM when displacing corner atoms is discussed in the Supplementary Materials.

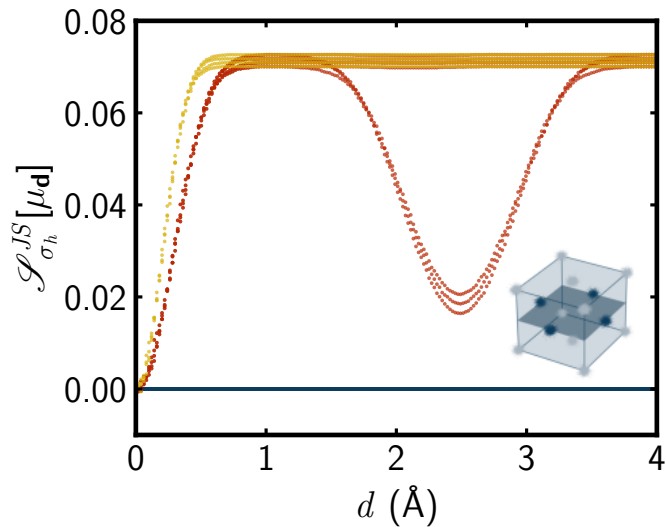


Figure 4: The SBM  $\mathcal{S}_{\sigma_h}^{JS}[\mu_d]$  of a cubic cutout from the Nickel structure when one of its in-plane atoms (darker blue atoms) is shifted parallel to the plane (blue), deviated from the plane by 45 degrees (red), or perpendicular to the plane (yellow). The SBM is calculated for the reflection operation  $\sigma_h$ , whose mirror plane passes through the center of the finite cluster, with its normal vector along the positive  $z$ -axis. The figure is plotted as a function of the length of the atom displacement  $d$ .

**Deviation from the reflection operator  $\sigma_h$**  We now consider SBM changes for the reflection operation  $\sigma_h$ , where the mirror plane passes through the center of mass of the finite cluster and its normal vector points towards the positive  $c$ -axis.

For an atom lying in the reflection plane atom, when the displacement is parallel to the mirror plane,  $\mathcal{S}_{\sigma_h}[\mu_d] = 0$  regardless of the displacement magnitude  $d$ , which is consistent with the blue curve in Fig. 4.

In contrast, when displacing an in-plane atom orthogonally to the mirror plane (as depicted by the yellow curve),  $\mathcal{S}_{\sigma_h}^{JS}[\mu_d]$  increases and rapidly converges, reaching a value of approximately 0.072 when  $d = 0.60$  Å. In this case the SBM reaches its disjoint plateau at a value of  $D$ .

When considering a displacement vector angled at 45 degrees from the plane (as illustrated by the red curve), in scenarios of small  $d$  values,  $\mathcal{S}_{\sigma_h}^{JS}[\mu_d]$  primarily depends on the  $c$ -component of the displacement vector. Thus the curve rises more slowly and reaches the plateau at  $\cos\theta D$ , where  $\theta$  is the angle the displacement vector makes with the reflection plane normal.

The behavior of  $\mathcal{S}_{\sigma_h}^{JS}[\mu_d]$  for small displacements is shown in Fig. 5. In this figure we also show the curves obtained by multiplying  $d$  by  $\cos\theta = 1/\sqrt{2}$ . The scaled curves lie on top of each other as expected, showing that it is just the  $c$  component of the displacement that contributes to the SB.

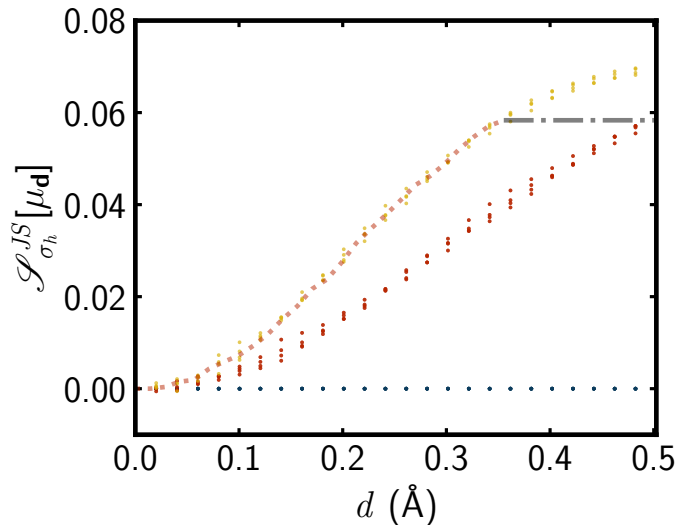


Figure 5: The SBM  $\mathcal{S}_{\sigma_h}^{JS}[\mu_d]$  of a cubic cutout from the Nickel structure when one of its in-plane atoms (darker blue atoms) is shifted parallel to the plane (blue), deviated from the plane by 45 degrees (red), or perpendicular to the plane (yellow). The SBM is calculated with respect to the reflection operation  $\sigma_h$ , whose mirror plane passes through the center of the finite cluster, with its normal vector along the positive  $c$ -axis. The figure is plotted as a function of the length of the atom displacement  $d$  and focuses on smaller displacement magnitudes. The left-side red curve is derived by compressing the  $d$ -axis of the right-hand side red curve by a factor of  $\sqrt{2}$ .

As before, some atoms exhibit the anomalous reduction in SBM at large displacements. For instance, when an in-plane atom is displaced towards and overlaps one of its closest corner atoms, a local minimum is observed at  $d = 2.49 \text{ \AA}$ , characterized by  $\mathcal{S}_{\sigma_h}^{JS}[\mu_d] = 0.018$ . Further discussion can be found in Supplementary Materials. Moreover, an analysis of the sample size utilized for calculating the SBM is also available in the Supplementary Materials for further reference, as well as some computational details about computing the measure.

## 5.2 The violation of symmetry elements of local distorted perovskites from rotations of rigid units

Here we consider a SB by a collective displacement of multiple atoms. For example, this might include the case of a second order structural phase transition due to a soft phonon mode.

**Test Design** For a concrete case, we consider the perovskites, a material class with nominal stoichiometry  $ABX_3$ . Due to their structural geometry that is well approximated as corner-shared rigid octahedra, the octahedra can collectively tilt in several different patterns, which can be described using a  $2 \times 2 \times 2$  (or smaller) supercell of the cubic perovskite unit cell, as described in Glazer’s classification [7] of allowed tilt patterns. For simplicity, we consider here a tilt system where an octahedron has no tilt around the  $a$  and  $b$  axes and only allows for a non-zero in-phase tilt around the  $c$  axis, corresponding to the tilt pattern  $a^0a^0c^+$  (No. 21 tilt system) in Glazer’s classification [7]. However, it serves our purpose as it allows us to explore the effect of collective rotations on the SBM.

The collective rotations are modeled using algebraic expressions that link displacements of atoms so as to preserve the rigid linked octahedral rotations. We have employed similar algebraic expressions previously for data simulation [21]. Specifically we consider  $\text{CaTiO}_3$  and use crystallographically reasonable  $U_{iso}$  values of  $0.0052 \text{ \AA}^2$ ,  $0.0027 \text{ \AA}^2$ , and  $0.0104 \text{ \AA}^2$  for Ca, Ti and O, respectively. The lattice parameter of the undistorted cubic perovskite is  $3.91 \text{ \AA}$ . Illustrations of this in-phase tilt pattern, as viewed down each tilt axis, are shown in Figure 6.

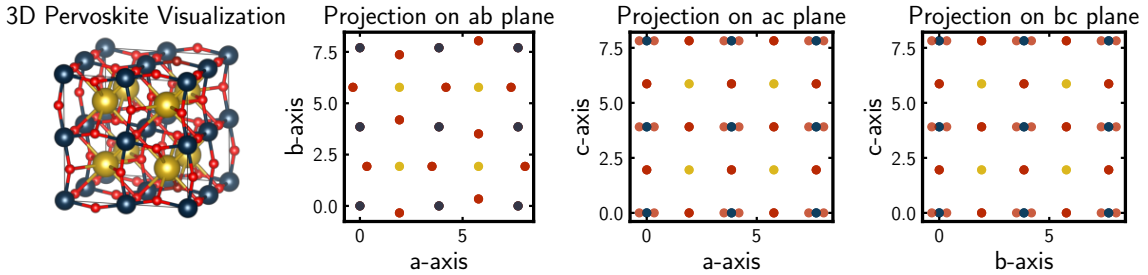


Figure 6: Visualization of an in-phase tilt systems projected along the three crystallographic axes in the  $2 \times 2 \times 2$  supercell, with a tilt angle of  $\phi = 10^\circ$ . The distortion corresponds to the  $a^0a^0c^+$  (No. 21 tilt system) in Glazer’s classification. In the representation, Ca cations are yellow, Ti cations are blue, and O are red. All dots are uniformly scaled to enhance clarity in the spatial distribution of the cations.

**SBM of the  $C_4$ , symmetry operator** As this distortion process occurs, the space group changes from  $Pm\bar{3}m$  (No. 221) to  $P4/m\bar{b}m$  (No. 127). Several symmetry operations that the tilted perovskite  $\mu_\phi$  breaks and preserves are tested, and the evolution of the SBM  $\mathcal{S}_\phi^{JS}[\mu_\phi]$  is analyzed as the tilted angle around the  $c$  axis,  $\phi$ , increases from 0 to 20 degrees.



First, we investigate the SBM  $\mathcal{S}_{C_4}^{JS}[\mu_\phi]$  associated with the four-fold rotation symmetry, and the results are illustrated in Fig. 7(a). The operator’s axis intersects the central Ti cation and is oriented along the  $a$  axis (represented by the blue curve),  $b$  axis (red curve), and  $c$  axis (yellow curve). As the octahedral tilt increases, the  $\mathcal{S}_{C_4}^{JS}[\mu_\phi]$  for  $C_4$  rotation along the  $c$  axis remains constant, as evidenced by the unvarying zero value depicted by the yellow line in Figure 7(a). Conversely, the transition from the space group  $Pm\bar{3}m$  (No. 221) to  $P4/mbm$  (No. 127) results in the disruption of  $C_4$  symmetry along both the  $a$  and  $b$  axes. By symmetry,  $\mathcal{S}_{C_4}^{JS}[\mu_\phi]$  of  $C_4$  along these two axes exhibit identical patterns of SB, as shown in the figure, where the  $\mathcal{S}_{C_4}^{JS}[\mu_\phi]$  for  $C_4$  rotation along the  $a$  axis (blue curve) and the  $b$  axis (red curve) display congruent monotonically increasing trajectories.

**SBM of the reflection operator,  $\sigma_h$**  The reflection plane intersects the central Ti cation, with its normal vector oriented towards the  $a$  axis (illustrated by the blue curve),  $b$  axis (red curve), and  $c$  axis (yellow curve), as depicted in Figure 7(b). Since there are no octahedral tilts around the  $a$  and  $b$  axes, reflection symmetry across the plane perpendicular to the  $c$  axis is preserved. This is consistent with the yellow curve remaining at zero independent of  $\phi$ , indicating the preservation of this symmetry under this distortion. Conversely,  $\sigma_h$  symmetry is disrupted over planes perpendicular to both the  $a$  and  $b$  axes, as reflected in the overlapping red and blue curves in Figure 7(b). Notably,  $\mathcal{S}_{\sigma_h}^{JS}[\mu_\phi]$  converges to approximately 0.24 beyond  $\phi = 13$ . Prior to  $\phi = 10$ ,  $\mathcal{S}_{\sigma_h}^{JS}[\mu_\phi]$  exhibits a more rapid increase compared to  $\mathcal{S}_{C_4}^{JS}[\mu_\phi]$  and is strictly larger. However, post  $\phi = 10$ ,  $\mathcal{S}_{C_4}^{JS}[\mu_\phi]$  accelerates in growth, while  $\mathcal{S}_{\sigma_h}^{JS}[\mu_\phi]$  approaches convergence, thus making  $\mathcal{S}_{C_4}^{JS}[\mu_\phi]$  greater than  $\mathcal{S}_{\sigma_h}^{JS}[\mu_\phi]$  for larger rotations. Consequently, the SBM analysis suggests that for smaller values of  $\phi$ , the octahedral tilts  $a^0a^0c^+$  predominantly disrupt the reflection over planes perpendicular to the  $a$  and  $b$  axes, compared to rotation around these axes, whereas for larger  $\phi$  values, the inverse is observed.

**SBM of the inversion operator,  $i$**  Since the octahedral tilts do not disrupt the inversion symmetry,  $\mathcal{S}_i^{JS}[\mu_\phi]$  maintains a value of zero for all  $\phi$  as expected, illustrated by the constant line in Figure 7(c).

## 6 Availability of code

The code for calculating the SBM is available as a Python-based open package in the following repository: <https://github.com/diffpy/diffpy.sbm>. The package is user-friendly, and detailed instructions for calculating the SBM for any finite cluster are provided in the repository’s README. Users can easily define their own finite clusters, or if working with crystals, the package supports importing unit cell data from a CIF file. Once the finite cluster is defined, you can apply distortions and calculate the SBM for various symmetry operations, such as rotation, reflection, inversion, and more.

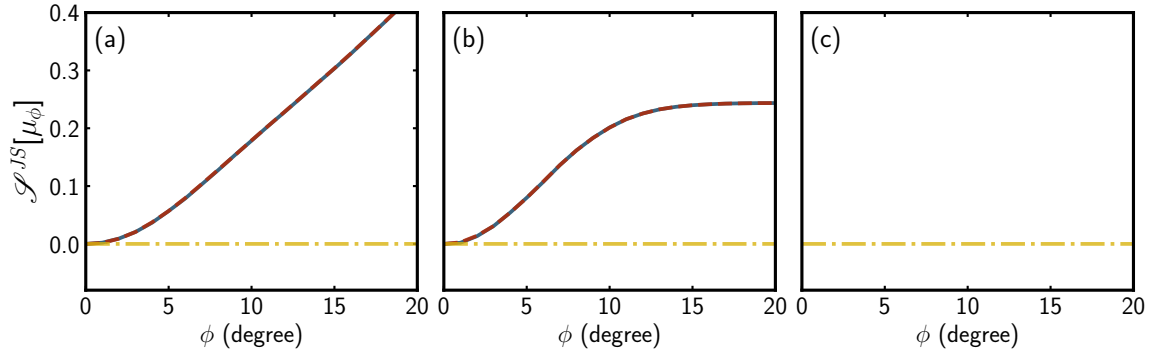


Figure 7: The SBM  $\mathcal{S}^{JS}[\mu_\phi]$  of a perovskite with in-phase octahedral rotations about an axis along the  $c$  axis. (a)  $\mathcal{S}_{C_4}^{JS}[\mu_\phi]$  is plotted for the four-fold rotation operator whose axis passes through the center Ti cation and points towards the  $a$  axis (blue curve), the  $b$  axis (red curve), and the  $c$  axis (yellow curve). (b)  $\mathcal{S}_{\sigma_h}^{JS}[\mu_\phi]$  is plotted for the reflection operator  $\sigma_h$ , whose mirror plane passes through the center Ti cation and is perpendicular to the  $a$  axis (blue curve), the  $b$  axis (red curve), and the  $c$  axis (yellow curve). (c)  $\mathcal{S}_i^{JS}[\mu_\phi]$  is plotted for the inversion operator  $i$ , whose fixed point is the central Ti cation. The figure is plotted as a function of the rotation angle  $\phi$  in degree.

Additionally, the code used to produce the results shown in this paper is publicly accessible at the GitHub repository: <https://github.com/lanikaling/SymmetryBreakingMeasure>, allowing readers to replicate the results or use it as a reference for their own work.

## 7 Conclusion

In this paper, we introduce a continuous SBM using the Jensen-Shannon divergence to analyze structural transformations and distortions. It is designed for studying SB in finite clusters where SB is continuous and there is value in quantifying it. In crystals, a symmetry is either present or broken, and it cannot be slightly broken. The continuous SBM, on the contrary, provides insights into local SB that would otherwise be obscured in the analysis of the infinite crystal.

Typically, for a finite cluster undergoing collective displacements of multiple atoms, traditional methods can only determine which symmetries are preserved or disrupted, without providing a comparative assessment of the extent of SB across different symmetry operations. In contrast, our SBM has proven to be a robust tool that can offer a quantitative framework for evaluating and comparing the degree of SB caused by various distortions. This approach not only identifies which specific symmetry operation experiences greater violation due to the distortion but also enriches the descriptive language available for quantitatively discussing structural distortions.

In recent years, with the growing application of machine learning (ML) in structural science [2], quantifying and implementing SB has become essential for identifying and discovering symmetries. In supervised tasks like symmetry discovery, this can involve either determining a numerical label that describes the symmetries of

the input dataset or incorporating SB directly into the loss function. For example, Forestano *et al.* [5] treat symmetry labeling as a black-box regression problem, while Liu *et al.* [16] incorporate symmetry into the loss function by quantifying SB as the violation of certain partial differential equations. Our SBM is well-suited for quantifying SB in these cases, as it is computationally efficient, applies to any finite cluster, and accounts for not only particle positions but also particle type and thermal vibrations. Additionally, in ML models for material prediction, SBM can serve as a bounded regularization term to enforce preferred symmetries.

## Acknowledgment

Work in the Billinge group was supported by U.S. Department of Energy, Office of Science, Office of Basic Energy Sciences (DOE-BES) under contract No. DE-SC0024141. The work of Qiang Du is supported in part by No. DE-SC0022317 and No. DE-SC0025347 from the Department of Energy.

## References

- [1] Henryk Arodz, Jacek Dziarmaga, and Wojciech Hubert Zurek, editors. *Patterns of Symmetry Breaking*. Springer Netherlands, Dordrecht, 2003.
- [2] Simon J. L. Billinge and Thomas Proffen. Machine learning in crystallography and structural science. *Acta Crystallographica Section A Foundations and Advances*, 80(2):139–145, March 2024.
- [3] E. S. Bozin, H. Xie, A. M. M. Abeykoon, S. M. Everett, M. G. Tucker, M. G. Kanatzidis, and S. J. L. Billinge. Local Sn Dipolar-Character Displacements behind the Low Thermal Conductivity in SnSe Thermoelectric. *Physical Review Letters*, 131(3):036101, July 2023.
- [4] Y. N. Fang, G. H. Dong, D. L. Zhou, and C. P. Sun. Quantification of Symmetry. *Communications in Theoretical Physics*, 65(4):423–433, April 2016.
- [5] Roy T Forestano, Konstantin T Matchev, Katia Matcheva, Alexander Roman, Eyup B Unlu, and Sarunas Verner. Deep learning symmetries and their Lie groups, algebras, and subalgebras from first principles. *Machine Learning: Science and Technology*, 4(2):025027, June 2023.
- [6] Punit Gandhi, Maria-Veronica Ciocanel, Karl Niklas, and Adriana T. Dawes. Identification of approximate symmetries in biological development. *Philosophical Transactions of the Royal Society A: Mathematical, Physical and Engineering Sciences*, 379(2213):20200273, November 2021.
- [7] A. M. Glazer. The classification of tilted octahedra in perovskites. *Acta Crystallographica Section B*, 28(11):3384–3392, 1972.

- [8] David J. Gross. The role of symmetry in fundamental physics. *Proceedings of the National Academy of Sciences*, 93(25):14256–14259, December 1996.
- [9] John R. Hershey and Peder A. Olsen. Approximating the Kullback Leibler Divergence Between Gaussian Mixture Models. In *2007 IEEE International Conference on Acoustics, Speech and Signal Processing - ICASSP '07*, volume 4, pages IV–317–IV–320, April 2007.
- [10] Julian Ivanov and Gerrit Schüürmann. Simple Algorithms for Determining the Molecular Symmetry. *Journal of Chemical Information and Computer Sciences*, 39(4):728–737, July 1999.
- [11] Shahar Keinan and David Avnir. Continuous Symmetry Analysis of Tetrahedral/Planar Distortions. Copper Chlorides and Other AB<sub>4</sub> Species. *Inorganic Chemistry*, 40(2):318–323, January 2001.
- [12] Shahar Keinan and David Avnir. Studies in copper(II) complexes: Correlations between quantitative symmetry and physical properties. *Journal of the Chemical Society, Dalton Transactions*, (6):941–947, 2001.
- [13] T. W. B. Kibble. Spontaneous symmetry breaking in gauge theories. *Philosophical Transactions of the Royal Society A: Mathematical, Physical and Engineering Sciences*, 373(2032):20140033, January 2015.
- [14] S. Kullback and R. A. Leibler. On Information and Sufficiency. *The Annals of Mathematical Statistics*, 22(1):79–86, 1951.
- [15] J. Lin. Divergence measures based on the Shannon entropy. *IEEE Transactions on Information Theory*, 37(1):145–151, January 1991.
- [16] Ziming Liu and Max Tegmark. Machine Learning Hidden Symmetries. *Physical Review Letters*, 128(18):180201, May 2022.
- [17] Klaus Mainzer. *Symmetries of Nature: A Handbook for Philosophy of Nature and Science*. Walter de Gruyter, Berlin ; New York, 1996.
- [18] Frank Nielsen and Ke Sun. Guaranteed Bounds on Information-Theoretic Measures of Univariate Mixtures Using Piecewise Log-Sum-Exp Inequalities. *Entropy*, 18(12):442, December 2016.
- [19] Leandro Pardo. *Statistical Inference Based on Divergence Measures*. Chapman and Hall/CRC, 1 edition, 2005.
- [20] Xiangyun Qiu, Th. Proffen, J. F. Mitchell, and S. J. L. Billinge. Orbital Correlations in the Pseudocubic O and Rhombohedral R Phases of LaMnO<sub>3</sub>. *Physical Review Letters*, 94(17):177203, May 2005.
- [21] Sandra Helen Skjærvø, Martin A. Karlsen, Riccardo Comin, and Simon J. L. Billinge. Refining perovskite structures to pair distribution function data using collective Glazer modes as a basis. *IUCrJ*, 9(5):705–712, September 2022.

- [22] Atsushi Togo, Kohei Shinohara, and Isao Tanaka. Spglib: A software library for crystal symmetry search. *Science and Technology of Advanced Materials: Methods*, 4(1):2384822, December 2024.
- [23] K. N. Trueblood, H.-B. Bürgi, H. Burzlaff, J. D. Dunitz, C. M. Gramaccioli, H. H. Schulz, U. Shmueli, and S. C. Abrahams. Atomic Displacement Parameter Nomenclature. Report of a Subcommittee on Atomic Displacement Parameter Nomenclature. *Acta Crystallographica Section A*, 52(5):770–781, 1996.
- [24] Inbal Tuvi-Arad, Yaffa Shalit, and Gil Alon. CSM Software: Continuous Symmetry and Chirality Measures for Quantitative Structural Analysis. *Journal of Chemical Information and Modeling*, 64(14):5375–5380, July 2024.
- [25] G. V. Vstovsky. Transform information: A symmetry breaking measure. *Foundations of Physics*, 27(10):1413–1444, October 1997.
- [26] B. E. Warren. *X-Ray Diffraction*. New York : Dover Publications, dover edition, 1990.
- [27] Hongyao Xie, Emil S. Bozin, Zhi Li, Milinda Abeykoon, Soham Banerjee, James P. Male, G. Jeffrey Snyder, Christopher Wolverton, Simon J. L. Billinge, and Mercouri G. Kanatzidis. Hidden Local Symmetry Breaking in Silver Diamondoid Compounds is Root Cause of Ultralow Thermal Conductivity. *Advanced Materials*, 34(24):2202255, 2022.
- [28] Hagit Zabrodsky, Shmuel Peleg, and David Avnir. Continuous symmetry measures. *Journal of the American Chemical Society*, 114(20):7843–7851, September 1992.
- [29] Xin-Gang Zhao, Oleksandr I. Malys, Simon J. L. Billinge, and Alex Zunger. Intrinsic local symmetry breaking in nominally cubic paraelectric BaTiO<sub>3</sub>. *Physical Review B*, 105(22):224108, June 2022.

# Supplemental Materials

## Section 3.2.2

Let  $F$  and  $G$  be two three-dimensional normal variables with means separated by vector  $\mathbf{d}$  and identical covariance matrices  $U\mathbf{I}_3$ , where  $U > 0$  is a constant. Their probability density functions are:

$$f(\mathbf{x}) = \mathcal{N}(\mathbf{x}; \boldsymbol{\mu}, U\mathbf{I}_3), \quad g(\mathbf{x}) = \mathcal{N}(\mathbf{x}; \boldsymbol{\mu} + \mathbf{d}, U\mathbf{I}_3). \quad (18)$$

### KL Divergence Calculation

The Kullback-Leibler divergence for two  $n$ -dimensional normal distributions  $u$  and  $v$  with means  $\boldsymbol{\mu}^u$  and  $\boldsymbol{\mu}^v$ , and covariance matrices  $\boldsymbol{\Sigma}^u$  and  $\boldsymbol{\Sigma}^v$  respectively, is given by [19]:

$$D_{\text{KL}}(u||v) = \frac{1}{2} \log \frac{|\boldsymbol{\Sigma}^v|}{|\boldsymbol{\Sigma}^u|} + \frac{1}{2} \text{Tr}((\boldsymbol{\Sigma}^v)^{-1}\boldsymbol{\Sigma}^u) + \frac{1}{2} (\boldsymbol{\mu}^u - \boldsymbol{\mu}^v)^\top (\boldsymbol{\Sigma}^v)^{-1} (\boldsymbol{\mu}^u - \boldsymbol{\mu}^v) - \frac{n}{2}. \quad (19)$$

For our case, since the covariance matrices are identical and equal to  $U\mathbf{I}_3$ , the formula simplifies as follows:

$$D_{\text{KL}}(f||g) = \frac{1}{2} \text{Tr}(\mathbf{I}_3) + \frac{1}{2U} |\mathbf{d}|^2 - \frac{3}{2} = \frac{d^2}{2U}, \quad (20)$$

where  $d = \|\mathbf{d}\|_{L_2}$  is the displacement distance.

## Section 5.1.2

### Deviation from four-fold rotational symmetry $C_4$

**SBM with displacements on corner atoms** In Figure 8, the displacement dynamics of one of the corner atoms within the nickel unit cell are examined. When the corner atom moves in a direction that does not interfere with other atoms in the lattice, the SBM  $\mathcal{S}_{C_4}^{JS}[\mu_d]$  rapidly converges to 0.143 ( $\approx 2/14$ ). This convergence value matches that observed for face atoms, suggesting a uniform threshold in the SBM associated with deviations from a  $C_4$  rotational symmetry in the context of a single atom displacement within this nickel unit cell. Additionally, a local minimum at  $d = 2.49 \text{ \AA}$  is identified, which is indicative of a scenario where a corner atom overlaps with its adjacent face atom. Further analysis anticipates the presence of additional local minima at  $d = 3.52 \text{ \AA}$ ,  $d = \sqrt{2} \times 3.52 \approx 4.98 \text{ \AA}$ , and  $d = \sqrt{3} \times 3.52 \approx 6.10 \text{ \AA}$ , which correspond to other significant lattice configurations, where the displaced corner atom aligns with other critical points in the unit cell.

### Deviation from the reflection operator $\sigma_h$

**SBM with displacements on out of plane atoms** We consider the more general case of out-of-plane atoms. As illustrated in Fig. 9, the response of  $\mathcal{S}_{\sigma_h}^{JS}[\mu]$  to atomic

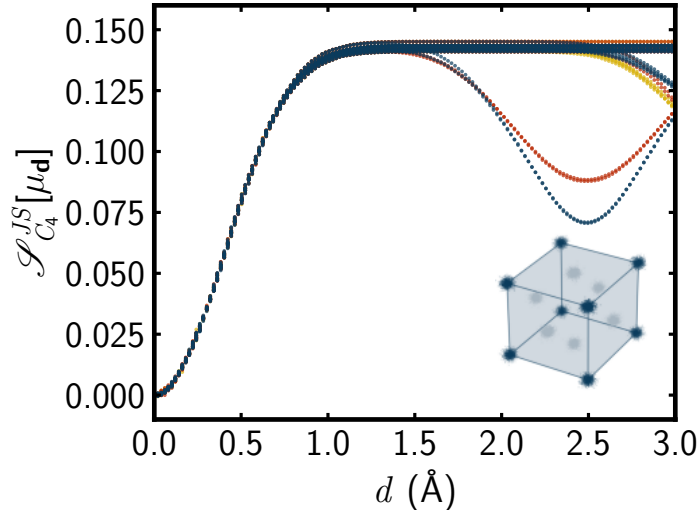


Figure 8: The SBM  $\mathcal{S}_{C_4}^{JS}[\mu_d]$  of a cubic cutout from the distorted Nickel structure. One of its corner atoms (darker blue atoms) is shifted parallel to the a-b plane (blue), deviated from the a-b plane by 45 degrees (red), or perpendicular to the a-b plane (yellow). The SBM is calculated for the four-fold rotational operation  $C_4$ , whose axis passes through the center of the finite cluster, with its direction along the positive c-axis. The figure is plotted as a function of the length of the atom displacement  $d$ .

displacements oriented parallel, at a 45-degree angle, and perpendicular to the mirror plane coincide for small  $d$ . The  $\mathcal{S}_{\sigma_h}^{JS}[\mu]$  corresponding to parallel distortion (depicted in yellow) achieves a local minimum of 0.072 at  $d = 1.76 \text{ \AA}$ . This coincides with scenarios where one of the out-of-plane atoms intersects the reflection plane. For the  $\mathcal{S}_{\sigma_h}^{JS}[\mu]$  subjected to a 45-degree angle distortion (represented in red), a local minimum of 0.072 is observed at  $d = 2.49 \text{ \AA}$ . This value is approximately  $\frac{\sqrt{2}}{2} \times 3.52 \text{ \AA} \approx 2.49 \text{ \AA}$ . This scenario mirrors the former, where a corner atom intersects the reflection plane. Lastly, the  $\mathcal{S}_{\sigma_h}^{JS}[\mu]$  with a parallel angle distortion (depicted in blue) attains its local minimum at a proximate  $d = 2.49 \text{ \AA}$ , registering a value of 0.091. This is indicative of a situation wherein one of the center out-of-plane atoms overlaps with one of its adjacent corner atoms.

**Sample size analysis** We make a note here to highlight certain numerical intricacies encountered during our tests. As discussed, we employ a Monte Carlo simulation to estimate the SBM. We found that the sample size required to obtain an estimate of the SBM at a certain level of accuracy increases as  $T_\alpha[\mu]$  deviates further from  $\mu$ . This implies that as atomic displacements magnify, Monte Carlo calculations demand more extensive sample sizes to yield estimates of SBM with consistent precision. In Fig. 10, we plot the sample sizes we used to estimate  $\mathcal{S}_{\sigma_h}^{JS}[\mu]$ . These sizes were determined considering a 95% confidence interval and a bilateral error tolerance of 0.0025. The procedure for computing the sample size is delineated in Algorithm 2.

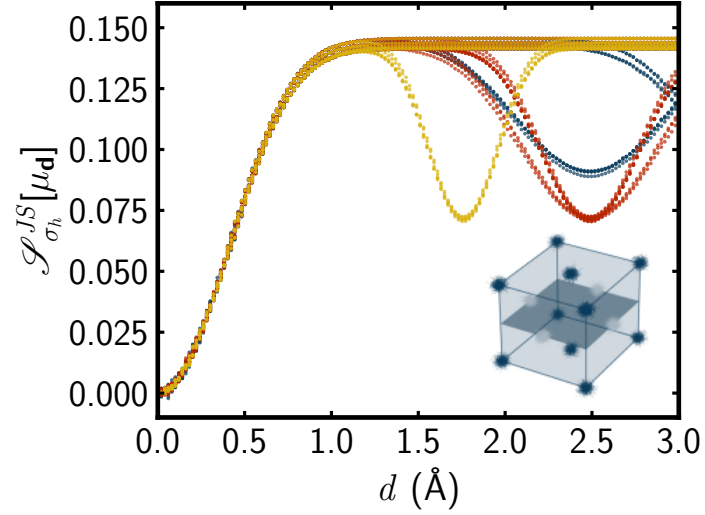


Figure 9: The SBM  $\mathcal{S}_{\sigma_h}^{JS}[\mu_d]$  of a cubic cutout from the Nickel structure when one of its out-of-plane atoms (darker blue atoms) is shifted parallel to the plane (blue), deviated from the plane by 45 degrees (red), or perpendicular to the plane (yellow). The SBM is calculated for the reflection operation  $\sigma_h$ , whose mirror plane passes through the center of the finite cluster, with its normal vector along the positive  $z$ -axis. The figure is plotted as a function of the length of the atom displacement  $d$ .

All the simulation tests addressed in this subsection employ a sample size determined through this methodology.



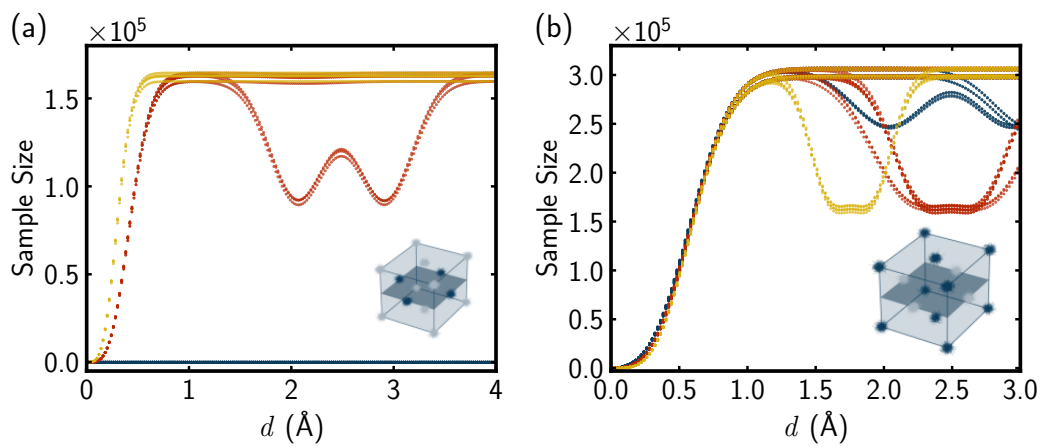


Figure 10: The recommended sample size for Monte Carlo simulations of  $\mathcal{S}_{\sigma_h}^{JS}[\mu]$ . The sample size for (a) finite clusters with displacements of in-plane atoms and (b) for displacements of out-of-plane atoms. The colors of the curves indicate the sample size for displacements parallel to the plane (blue), 45 degrees to the plane (red), and perpendicular to the plane (yellow). These were the sample sizes needed to give  $\mathcal{S}_{\sigma_h}^{JS}[\mu]$  with a 95% confidence interval and an error tolerance of .0025 on each side.